Light Metals 2013 *Edited by: Barry Sadler*
TMS (The Minerals, Metals & Materials Society), 2013

REDUCED VENTILATION OF UPPER PART OF ALUMINUM SMELTING POT: POTENTIAL BENEFITS, DRAWBACKS, AND DESIGN MODIFICATIONS

Ruijie Zhao[1,2], Louis Gosselin[1], Mario Fafard[2], Donald P. Ziegler[3]

[1]Aluminium Research Centre-REGAL and Departement of Mechanical Engineering, Université Laval, Québec City, Québec, Canada, G1V 0A6
[2]NSERC/Alcoa Industrial Research Chair MACE[3] and Aluminium Research Centre-REGAL, Université Laval, Québec City, Québec, Canada, G1V 0A6
[3]Alcoa Canada Primary Metals, Aluminerie Deschambault, Deschambault-Grondines, Québec, Canada, G0A 1S0

Keywords: aluminum smelting pot, energy efficiency, fan power, CFD, ventilation reduction

Abstract

Maintaining current draft conditions in the upper part of Al smelting cell requires important electricity consumption for the fans. A reduction of the ventilation rate could significantly diminish the total power requirement at the blowers. However, adverse changes in operating conditions due to this ventilation reduction may disrupt the pot thermal equilibrium. A CFD model was created to investigate the influence of ventilation reduction on pot thermal balance. With the objective of maintaining normal heat losses by the top of the cell, several modifications are simulated, such as using plate fins on the anode assembly, changing hood gap geometry and modifying anode cover thickness. Heat transfer rates are determined for these modified designs, and compared to those currently achieved.

Introduction

Today's aluminum reduction technology is based on the Hall-Héroult process, which requires intensive energy input. Typically, ~13-15 MWh are required for producing 1 ton of Al, and roughly half of the energy input is lost from pots as waste heat. Due to the extensive amount of heat lost in the Al production industry, waste heat recovery has become a much researched topic in recent years. The "simplest" way to capture waste heat is from the pot exhaust gas which contains ~35%-40% of the heat lost by pots. Sørhuus et al. [1] presents the design of a heat exchanger (HEX) for cooling the collected pot gases and thus recovering heat from them. Fouling on the HEX surfaces was analyzed and it was found that an annual cleaning was sufficient to maintain a proper heat transfer in the HEX even though the pot exhaust is largely contaminated with fouling agents. Fleer et al. [2] paid attention to the particle characteristics in the effluent, exhaust gas properties, and fouling propensity in the gas stream in front of the dry scrubber. The aforementioned works are mainly focused on current pot effluents, which are at a relatively low temperature (~100-130˚C). Such low energy grade limits the potential usage of the waste heat.

Several theoretical and experimental studies have shown that the cell ventilation condition has the most influence on the pot exhaust temperature and heat content. Based on reported measurements in Gadd's thesis [3], the exhaust temperature could increase by 50˚C when cell draft is reduced to 40% of the normal condition. Abbas [4] has determined the top heat losses in different draft conditions (i.e., from 3% to 160% of normal draft conditions) based on CFD simulations. This work shows that the pot effluents temperature can increase by over 100˚C as the draft condition decreases to 20% of normal conditions. This work also proposes some geometrical modifications of the smelting pot to enhance the thermal quality of the pot gases [5]. Lorentsen et al. [6] reported that Hydro (Norway) has developed a gas suction technology that collects the CO_2 close to the feed hole, yielding a warmer and more concentrated flue gas, with less fan power required. An increase of temperature means an enhancement of the thermal quality of the waste heat, while an increase of CO_2 concentration is desirable in view of CO_2 capture processes. Moreover, reducing the cell ventilation rate can reduce drastically the fan power requirement, since it is typically proportional to the flow rate to power 3 ($P_{fan} \sim Q^3$). For the sake of illustration, let us consider the fan energy consumption at a typical modern plant producing ~260,000 ton/y of Al. Two fans work to transport the flue gases to the gas treatment center, each with a power of 8467 kW, for a total annual electricity consumption as high as 148.3 GWh. Assuming 0.05 US$/kWh, the annual cost of electricity for fans would be 7.4 MUS$. If one can reduce the ventilation rate by half, the fan power can be roughly reduced to 1/8th of the normal consumption.

However, reducing pot ventilation may disturb current operating conditions. For instance, reduced ventilation means that less heat is extracted through the top section of the smelting pot [4, 7], and therefore, more heat has to be dissipated via sidewalls which could melt the frozen electrolyte and jeopardize pot integrity. Another aspect to be considered is the fume emissions from the pots to the potroom. A certain level of negative pressure should be maintained in the pots to prevent emissions to potroom.

In this work, we studied the heat transfer impacts of ventilation reduction in an Al smelting pot with CFD simulations. The model is based on actual pot design and operation. Different modifications are studied to overcome the adverse changes due to ventilation reduction. The objective of this work is to compare different scenarios in order to reduce the ventilation to a minimum level while maintaining current thermal equilibrium in the bath.

CFD Model

Simplifying Assumptions

The domain of interest is the upper section of an aluminum reduction cell, above the electrolytic bath. Several assumptions are made to reduce the computational burden:
(i) A typical 350kA aluminum cell contains 40 anodes, divided in two parallel rows. By imposing a negative pressure at exit, air in the potroom enters the domain through gaps between hoods,

around anode rods and other superstructure openings, and dilutes the CO_2 released by the Hall-Héroult process. The effluents are collected in a duct through 5 inlets located equidistantly on the bottom of the superstructure. Neglecting side effects and considering that the heat transfer and flow pattern is the same below each of the 5 inlets, only the domain above two anodes needs to be simulated, as shown in Fig. 1. Such a unit consists of two anodes, 1/4 feed hole, 1/4 duct inlet, and the corresponding anode cover, superstructure and hoods. The flow pattern is periodic in the direction of the anodes row. This allows simulating only $1/20^{th}$ of a pot.

(ii) The bottom boundaries of the simulated domain are the immersed part of the anodic blocks and the bottom surface of crust. The CO_2 layer due to the accumulation of the hot gas emissions from the bath is not included. Here, we estimated the mass flow rate of the hot gas and imposed it as a mass inflow to the domain at the feed hole.

(iii) A typical new anode has a height of ~0.6 m, and it is consumed to ~0.15 m before removal from the pot. The heat transfer rate through an anode varies strongly during anode consumption. However, since each pot contains 40 anodes at different levels of consumption, an average height of 0.4 m was assumed for the anodic blocks.

(iv) A part of the potroom and upper cavity neighboring to the superstructure and hoods was included in the domain with an extended length of 0.5 m. The infiltration of air in the cavity under hoods comes from the gaps between hoods. Other very narrow gaps were ignored in the model. The gap width is 1 cm.

Governing Equations

The governing equations are those expressing the conservation of mass, momentum in each direction, energy, and electrical charge. Reynolds-Averaged Navier-Stokes (RANS) equations are applied to simulate the turbulent flow. Incompressible fluid flow and steady-state conditions are considered. Pressure work and kinetic energy terms are neglected in the energy equation. Viscous heating is also ignored. Note that in the solids, only the energy and electrical charge equations are solved. All properties were assumed to vary with temperature and the equations are available in the Ansys Fluent documentation [8]. As for heat transfer by radiation, the gas is treated as a non-participating medium. Only surface-to-surface radiation heat exchange is involved in the CFD, and is calculated with the Discrete Ordinates (DO) Radiation Model [8], which can be run in parallel. All surfaces corresponding to inlets and outlets are treated as blackbodies.

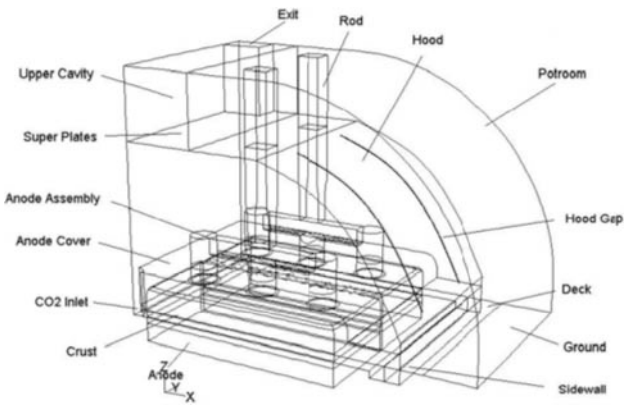

Figure 1. Schematic view of the domain of the CFD model.

Turbulence Model

The RANS equations need a turbulence model to calculate the Reynolds stresses term. A proper choice of turbulence model is required to achieve an adequate tradeoff between accuracy and computational time. The airflow pattern in the cavity under the hoods shares many similarities with the induced airflow in enclosed environments (e.g., jet flow and impingement on a wall, and buoyancy-driven flow). Before 2005, the k-ε family of turbulence models was very popular in indoor environment simulation and a general conclusion is that overall the RNG k-ε model provides the best performance. Recently, the k-ω turbulence models have attracted more attention in industrial applications. A comprehensive review on validation of turbulence models was reported by Zhai et al. [9, 10]. They compared CFD simulations to experimental results. The RNG k-ε and SST k-ω have shown the best performance. In cases with strong natural convection and high-Reynolds number jet flow, the SST k-ω model provided better results. In the present problem, airflow at potroom temperature is induced into the cavity under hoods where the wall temperature can reach 200-300°C. Strong natural convection thus occurs between the walls and the airflow in the cavity [11] and for this reason the SST k-ω model was chosen.

Numerical Modeling and Mesh

The equations of the present model were solved with a CFD commercial software that relies on the finite volume approach [8]. Meshing of the domain was built so as to respect the requirements of the turbulence model. The SST k-ω model in the CFD software applies a two-layer zonal model to simulate the flow in the region close to the walls. However, to avoid first near-wall nodes in the buffer layer region, the near-wall meshes should ideally be either coarse ($y+>30$) or fine ($y+\approx 1$). Based on earlier work from Zhao [11], the wall function method (applied to coarse meshes) poorly describes the near wall region with low Reynolds number flows. The airflow in the present study is relatively weak and does not have a high Reynolds number near walls. Moreover, when reducing the pot draft condition, buoyancy will significantly influence the flow features. Therefore, a fine near-wall mesh is used.

The mesh is created in GAMBIT 2.4 and consists of prism volumes in the boundary layer and Tet/Hybrid volumes in the core of the domain. A mesh independence study is presented below. A typical mesh contained ~2.5 million control volumes. The SIMPLE algorithm was used to solve flow equations. Default criteria in the software were used to declare convergence of a simulation. The solution strategy relied on a step-by-step procedure. One can first launch the simulation with a low value of gravity, and converge it using first-order schemes. Following that the resulting physical fields are used as an initial guess for a new simulation in which gravity is adjusted properly. Similarly, second-order schemes could then be introduced. Approximately 24 hours were required for performing one simulation.

Boundary Conditions

Atmospheric pressure is imposed at the potroom boundary. The pressure at the exit (inlet of the collecting duct) was an adjustable negative pressure (−10 to −50 Pa). The exhaust draft condition can be varied by changing the inlet-to-outlet pressure difference, which is the sum of pressure losses through hood gaps and in the

cavity under hoods. To simulate the CO_2 emission from the bath into the cavity, the bottom surface of feed hole was defined as a mass inflow boundary from which hot gases (CO_2) are released at 940˚C with a mass flow rate of 2.6 g/s for our simulated domain (based on 1.3 vol% hot gas concentration in the pot effluents). Since the properties of CO_2 are close to those of air and the typical CO_2 concentration is just ~1-2% in the exhaust, we replaced the CO_2 gas with air to simplify the model. The turbulence intensity was set to 1% at all flow boundaries to indicate a low turbulent inflow. Turbulent viscosity ratio was fixed to 1 at the potroom boundary for simulating an external free flow [8]. The hydraulic diameter was used to define the turbulence at the mass inflow and outlet boundaries. Impermeability and no-slip flow are assumed on all other solid surfaces.

Convective heat transfer is imposed at the surface of anode blocks immersed in the bath, at the external surface of the sidewall and at the surface of deck and ground. The bath temperature was set at 955˚C. Combined external radiation and convection heat transfer is defined at the bottom surface of the crust and the surfaces of anode exposed in the CO_2 layer. The gas temperature representing CO_2 was 940˚C in the present simulations. The convection coefficient in the pseudo CO_2 layer was determined by an analysis presented in the next section. At the potroom boundary, the ambient temperature near the pot is set to 50˚C while the temperature is assumed to 70˚C at the boundary of upper cavity. Radiation between the pot surfaces and the far-field environment is also considered in the model. The background temperature in the potroom was 30˚C, and that for the upper cavity, 70˚C. On sidewalls, a heat transfer coefficient of 10 W/m^{2}K was considered with an ambient temperature of 100˚C. The emissivity of anode cover and crust were 0.4 and 0.3, respectively [12]. The emissivity of metal surfaces in the cavity was 0.8, while it was 0.5 at the surfaces outside the cavity [13]. Electrical insulation is imposed on all surfaces of the domain except for the top surface of rod where a current of 8500 A/rod is imposed, and the bottom of anodes with a zero voltage.

Verification and Validation

Values of y+ were verified on all wall boundaries. The value of y+ is equal to ~1 in the cavity under hoods and ~1-3 in the potroom and upper cavity, which satisfies the requirement of the enhanced wall function used in SST k-ω model. Also, the blending function, which is incorporated in the SST k-ω model and which controls the turbulent model transition between the standard k-ε model in the core area and the k-ω model in the near-wall regions, was looked at. It was found that the k-ε model was successfully applied in the areas of jet flow and the core space of the cavity, while the k-ω mode was activated in the area near wall surfaces.

Mesh independence was thoroughly investigated. Previous work by Zhao [11] showed that a maximum control volume length scale of 5 cm in the core area of flow domain is fine enough to capture the main heat transfer and flow patterns. However, a refined surface mesh is required in particular areas such as for the gaps and anode assembly. The bulk volumes are created based on the surface mesh and gradually grown to 5 cm (mesh#1, 2.45 million control volumes). A mesh with a maximum volume length scale of 3 cm was also created (mesh#2), with 3.98 million control volumes. Mesh#1 was compared to mesh#2 for both ventilation rates (i.e., normal 2.4 Nm^3/s, and reduced to 1.2 Nm^3/s). Results did not change significantly from mesh#1 to mesh#2 (Table I). Therefore, mesh#1 is considered adequate for the rest of this paper. An analysis was performed to determine proper values for some uncertain simulation parameters. For example, a series of simulations was performed with different distances from the surface of hoods to the potroom boundary. It was found that the mass flow rate and temperature of the exhaust, and the heat transfer rate from the bath did not change when the potroom domain was extended above 0.5 m. Another uncertain parameter was the convection heat transfer coefficient of the CO_2 gas under the crust. The dominant heat transfer mechanism in the cavity under crust is radiation (radiation heat transfer coefficient of ~100 W/m^{2}K [14]). Three different values of 5, 10 and 20 W/m^{2}K were assigned to the convection coefficient to test its influence and very little influence was found (e.g., 0.16% relative error in the total heat transfer rate from the bath). Therefore, we used a value of 10 W/m^{2}K in the rest of this work.

Table I. Comparison of CFD results with two meshes, for two ventilation conditions (shaded lines are for reduced ventilation).

Parameter	Mesh#1	Mesh#2	Relative error, %	Description
$\dot{m}_{gas}$ (kg / s)	0.1446	0.1452	0.41	Mass flow rate at exit
	0.0734	0.0733	0.14	
T_{gas} (˚C)	132.5	133.5	0.75	Gas average temp. at exit
	175.5	174.5	0.57	
T_{hood} (˚C)	138.5	138.5	0	Average temp. of hoods
	169.5	172.5	1.7	
p_{gap} (Pa)	−18.55	−18.75	1	Aver. pressure at gaps
	−4.28	−4.28	0	
q_{gas} (W)	15650	15800	0.95	Heat loss at exit
	11100	11050	0.45	
q_{bath} (W)	9100	9160	0.66	Heat transfer rate from bath
	8380	8360	0.24	

Top Heat Loss in Current Pots under Normal and Reduced Ventilation Rates

When reducing ventilation in the pot, one of the most adverse influences is the reduction of bath heat loss by the top of the cell. When that happens more heat will escape by the sidewalls, which is exactly where the protective ledge thickness is very sensitive to the heat flux. A higher heat flux may melt the inner frozen crust and narrow the lining thickness. Moreover, the crust strength over the side-channel could also be reduced due to the inner crust melting, which is likely to increase the area of collapsed open holes in the side-channel cover. Therefore, when reducing the ventilation of the cell, strategies should be developed in order to increase the top bath heat loss up to its "normal" value to avoid these negative impacts. In order to understand how the heat transfer changes in the domain due to ventilation reduction, a simulation was performed under normal ventilation (2.4 Nm^3/s) and another one, under reduced ventilation (50% of normal ventilation rate).

Figure 2 reports the heat transfer rate related to different components under the two ventilation scenarios considered. q_{bath} represents the total heat extracted from the bath through the top of

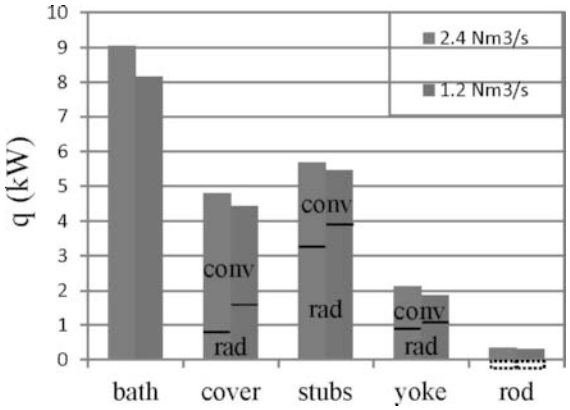

Figure 2. Heat losses due to convection and radiation from different components in different ventilation conditions.

the cell. q_{cover}, q_{stubs}, q_{yoke}, and q_{rod} represent respectively the total heat transfer rate that leaves the surface area of the cover, stubs, yoke and rod that is exposed to the gas in the cavity. Note that the total heat loss via the upper part of a pot consists of the heat extracted from bath (q_{bath}) and the heat generated by Joule heating in the anode and the anode assembly, which is why the summation of q_{cover}, q_{stubs}, q_{yoke}, and q_{rod} is larger than q_{bath}. Experiments [15] performed in a 75 kA prebaked cell have shown that under normal conditions ~76% of the heat leaves the domain in the exhaust gas and the rest (~24%) is being dissipated directly in the potroom environment via the surfaces of hoods and superstructures. The anode assembly (in particular, stubs and yoke) is responsible for most of the heat loss via the top of the cell, while there is also a significant portion escaping through the anode cover. When appropriate, a line separates the radiative and convective contributions in Fig. 2. For example, the heat loss from the top surface of anode cover (q_{cover}) is reduced from 4805 W to 4435 W when the ventilation flow is reduced by half. However, the radiative heat loss is actually increased by 755 W while the convective heat loss is attenuated by 1125 W. The rod surface is a special case where radiation is received and therefore the radiation heat transfer rate is a negative value (indicated by the dotted bars, in Fig. 2). The convective heat loss is actually the sum of the solid bar (net heat loss) and the dotted bar in each case.

When the ventilation flow is reduced by half, the total heat transfer rate extracted from bath by the top of the cell is decreased from 9040 W to 8165 W, i.e. a reduction of 875 W (in the two anodes model). In practice, this extra heat of 875 W would have to escape from other pot components. It is found that the heat losses from all surfaces are reduced somehow. And although the heat loss reduction by each surface seems relatively weak, their sum is large enough to potentially influence the overall pot thermal balance. Looking at Fig. 2, one can also conclude that convective heat losses are reduced in a less ventilated pot, while the radiation increases due to warmer surfaces. However, the overall enhanced radiative heat loss is not enough to compensate the reduction in convective heat loss. Convection is the main mechanism for heat loss from anode cover surface, while radiation dominates the heat loss from anode assembly surface.

Some conclusions can be drawn from the abovementioned analysis. These will help to design proper modifications to the pot in order to maintain thermal equilibrium under low ventilation scenarios:

(i) The convective heat loss in the cavity is decreased as the ventilation is reduced, while the raditive heat loss has the opposite behavior.

(ii) The enhanced radiative heat loss is not enough to compensate the reduction of convective heat loss due to ventilation reduction, and this is the main reason why the net top heat loss is reduced.

(iii) Radiation plays a significant role on the yoke and stubs for the two draft conditions. When ventilation is reduced, radiation becomes the most influencing mechanism in the top heat loss.

Three types of modifications are studied in the following sections to achieve proper thermal equilibrium (i.e., to extract from the bath the missing 875 W of heat mentioned previously): use of fins on the anode assembly, change of the gaps geometry, and change of anode cover geometry and surface properties.

Addition of Fins on Anode Assembly

The first group of scenarios is the addition of fins on the anode assembly. Plate fins were positioned on anode yoke and stubs, as shown in Fig. 3. The purpose of the fins is to increase the convective heat loss from the anode assembly to the airflow in the cavity. Traditionally, the design of fins involves an optimization of different design variables, e.g. fin dimensions, materials and arrangement. Here, we studied two designs (cases a1 and a2) to evaluate their efficiency in maintaining top heat loss under low flow of ventilation. We fixed the fin width and thickness at 5 cm and 1 cm, respectively. Fin material is steel (as yoke and stubs). Case a1 only has one plate fin, while case a2 has three plate fins. New meshes were built with the fins and CFD simulations were performed under reduced ventilation for these designs.

The influence of fins on the total heat transfer rate from bath is shown in Fig. 4. Compared to the 1.2 Nm^3/s ventilated situation with no fins (case_1/2), case a1 increases the heat transfer rate from the bath by 315W and case a2 by 385W, respectively (see Fig. 4). It is found that using one or three fins does not change significantly the net top heat losses. However, in both cases, there is still a significant gap for achieving the "normal" heat transfer rate dissipated via the top section under normal level of ventilation flow. The use of fins on anode assembly was thus found to be inadequate to fully compensate the reduction of top heat loss caused by such reduced ventilation flow.

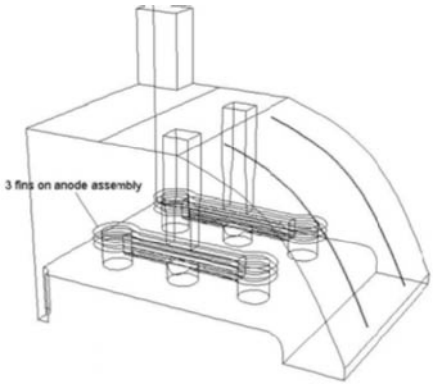

Figure 3. Schematic of fins addition on anode assembly (case a2).

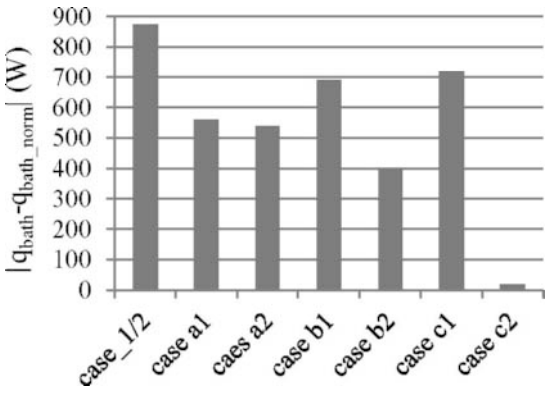

Figure 4. The difference of heat transfer rate extracted from bath by the top of the cell between normal condition and simulated scenarios.

In order to understand why such a result was achieved, the relative enhancement of convective and radiative heat losses from different components, for different scenarios, is presented in Table II. The reference case for this table is the 50% of normal ventilation case, without fins, namely case_1/2. Positive heat transfer rate indicates an enhancement with respect to case_1/2 while a negative value means reduction of heat transfer introduced by the geometrical modification. Table II indicates that on the one hand fins increase the convective heat loss on cover, stubs and yoke, while on the other hand the fins reduce the radiative heat loss from these components (cases a1 and a2). It can be explained by the fact that the fins on anode assembly block the radiation transfer from cover, yoke and stubs to other cold surfaces. Although the fins create more surface area, the overall effect on the radiation heat transfer is nevertheless negative. Therefore, fins alone were found to be poorly efficient, in particular when considering the complexity they would introduce in production and mechanical operations.

Modification of Hood Gaps Geometry

In the second group of scenarios, we considered to enhance the convection heat losses by increasing the induced airflow velocity from hood gaps (case b1) or by adopting a horizontal flow arrangement from hood gaps (case b2). In case b1, the flow velocity can be increased by reducing the total gap area (increasing the tightness of the pot). We assumed in the CFD model a uniform width of 1 cm for each gap. The gap area could be reduced by welding flaps on the edge of each hood to cover a part of the gap. It is obvious that the covering flaps cannot provide a perfect sealing on hood gaps. However, comparing with the mass flow rate though uncovered gaps, the leakage through flapped gaps could be neglected in the present model. In this scenario (b1, as shown in Fig. 5 on left), the upper half of each gap was assumed covered and therefore the flow velocity through the uncovered gap needs to be doubled in order to maintain the same mass flow rate through the pot. The results are shown in Fig. 4. It is found that there is still a ~700 W gap of the heat transfer rate from bath compared to normal operating conditions.

Even though the faster induced flow significantly increases the convection heat loss on anode cover, when comparing with case_1/2 there is a large sacrifice in the radiative heat loss from anode cover, as illustrated in Table II. In addition, the convective heat loss from the anode assembly is not significantly increased in

Table II. Convection and radiation heat transfer enhancement (in W) provided by different scenarios compared to case_1/2.

		case a1	case a2	case b1	case b2	case c1	case c2
cover	conv	325	262	687	624	71	402
	rad	−282	−258	−547	−503	90	−425
stubs	conv	421	599	180	610	63	464
	rad	−303	−371	−61	−406	−106	738
yoke	conv	241	258	-207	178	82	46
	rad	−141	−170	109	−99	−38	−272
rod	conv	−26	−28	−5	−10	7	12
	rad	−1	7	24	22	−21	−80

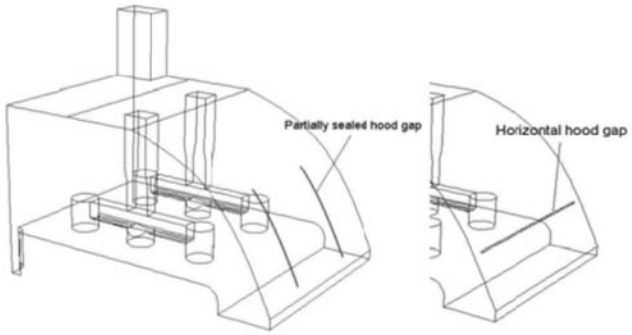

Figure 5. Schematics of sealed hood gaps (case b1, left) and horizontal hood gaps (case b2, right).

this case. The flow induced from the lower half gap is "trapped" in the side-channel which is formed by the height difference between the anodic block and the pot deck. Another negative effect is that the more tight pot structure introduces a significant increase on the driving pressure difference (i.e. from −10 Pa to −40 Pa) and would therefore need additional fan power to maintain 50% of normal ventilation. In the future, an optimization on the flow pattern could be helpful for the convection enhancement on the anode assembly.

To replace current vertical gaps, a horizontal gap was considered in case b2, as shown in Fig. 5 on right. With such geometry, the flow passes more efficiently over the anode cover and anode assembly. A horizontal gap on hoods was created in the CFD model and the gaps between hoods were covered by flaps as in case b1. From Fig. 4, we found that the heat transfer rate from bath was increased by ~475 W when compared with the 50% normal ventilation case. In other words, there is still ~400 W of heat extracted from the bath that is missing compared to normal conditions. Table II indicates that the convective heat losses from cover, stubs and yoke are distinctly enhanced by such flow arrangement. However, the overall enhancement of heat loss is attenuated by the reduction of radiation heat transfer on all three surfaces. This is due to the strong temperature-dependence of radiative emissions. A small surface temperature reduction induced by convection can result in a large radiative heat transfer reduction. In any case, both strategies b1 and b2 are not adequate enough to recover the reduction of top heat loss under the low ventilation condition studied here. And to add to that a reduction in the gap area will also induce a significant additional pressure difference to maintain the ventilation rate as it is.

Modifications on Anode Cover

For an opaque, diffuse, gray surface, the net radiative transfer is strongly influenced by the surface emissivity. When increasing the emissivity also the net radiation transfer of the surface will increase. For the normal condition the emissivity of the top surface of anode cover was assumed to be 0.4. In case c1 we assumed that the emissivity could be increased to 0.8 (e.g., a dust layer on the anode cover) and with that we performed the simulation without any other geometrical modification. By studying the results presented in Fig. 4 and Table II, the increase in terms of top heat loss was found to be limited: Only ~200 W additional heat is extracted and when compared to the low ventilation case without modification; there is still ~700 W that should be extracted in order to maintain current conditions.

When the ventilation flow is reduced to 50% of normal condition, the contribution from radiation in the top heat loss is larger than that of convection, as shown in Fig. 2. Since the addition of fins on anode assembly has proven to suppress the radiative heat transfer, one may think about enhancing the radiation heat loss rather than the convective heat loss. The radiative heat exchanges between surfaces are determined by surface emissivity and temperature, view factors and surface areas. Among these factors, view factor and surface area are strongly dependent on the pot geometry. In case c2, the idea tested consisted in exposing an additional segment of anode stubs (5 cm deep) in the cavity by removing some anode cover material surrounding the stubs, as shown in Fig. 6. In such a case, the deeper exposed stubs have a higher surface temperature which can increase both convection and radiation heat transfer from these surfaces. Meanwhile, the original configuration of anode assembly is maintained to avoid any interference of additional structure in the radiation heat exchanges in the cavity. Moreover, the anode cover still has a 5 cm thickness close to the stubs to prevent the anode from being burnt with the oxygen of the air. Results of the CFD simulations are shown in Fig. 4. The heat transfer rate from bath in case c2 is almost the same as that in the normal ventilation case. This strategy thus seems to have the potential to enhance the top heat loss to the normal level while the ventilation flow is reduced by half. By studying the detailed information of heat losses from different components in Table II, we found that the heat loss from the stubs is significantly enhanced, both by convection and radiation. The more exposed stubs with higher temperature (~500°C) can emit more radiation while convective heat loss is also increased as a result from more stubs in contact with the airflow in the cavity. Lastly, this modification will induce little effect on the total driving pressure between the gaps and exit.

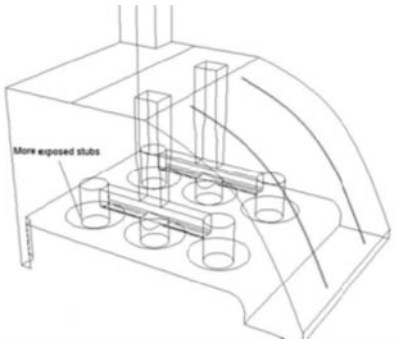

Figure 6. Schematic of more exposed stubs in the cavity (case c2).

Conclusions

Different advantages can be envisioned by a reduction of cell ventilation. However, it also creates thermal imbalance compared to current pot operation since less heat is removed from the bath by the top of the cell. A CFD model of the upper part of a typical cell was developed in order to investigate different scenarios. The objective was to find how to maintain the same amount of heat removed from the bath even when the ventilation is reduced. The most promising set-up found was to expose a larger portion of the stubs to the flow of air. In future work, different simultaneous combinations of the different scenarios could be investigated.

Acknowledgements

The authors acknowledge the financial support from REGAL (Aluminum Research Centre) for participating to the conference. This work was supported by the Fonds de recherche du Québec - Nature et technologies (FRQ-NT). Zhao's work was also supported by the Chinese Scholarship Council (CSC). The authors would like to thank Alcoa for its participation in this research.

References

[1] A. Sørhuus and G. Wedde, "Pot Gas Heat Recovery and Emission Control", *Light Metals 2009*, (2009), 281–286.

[2] M. Fleer et al., "Heat Recovery from the Exhaust Gas of Aluminum Reduction Cells," Light Metals 2010, (2010), 243-248.

[3] M. D. Gadd, "Aluminium Smelter Cell Energy Flow Monitoring" (Ph.D. thesis, University of Auckland, 2003).

[4] H. Abbas et al., "The Impact of Cell Ventilation on the Top Heat Losses and Fugitive Emissions in an Aluminium Smelting Cell", Light Metals 2009, (2009), 551-556.

[5] H. Abbas, "Mechanism of Top Heat Loss from Aluminium Smelting Cells" (Ph.D. thesis, University of Auckland, 2010).

[6] O. A. Lorentsen et al., "Handling CO2eq from an Aluminum Electrolysis Cell", Light Metals 2009, p. 263.

[7] R. Zhao et al., "Heat Transfer in Superstructure of Electrolytic Cells-Part I: Thermal Circuit and Sensitivity Analysis from a Waste Heat Recovery Standpoint", Applied Thermal Eng., (2012), (submitted).

[8] ANSYS FLUENT, "Ansys Fluent 12.0/12.1 Documentation," Users Guide Manual, Ansys Inc, 2009.

[9] Z. J. Zhai et al., "Evaluation of Various Turbulence Models in Predicting Airflow and Turbulence in Enclosed Environments by CFD: Part I—Summary of Prevalent Turbulence Models", HVAC&R Research, 2007, vol. 13, no. 6:853–870.

[10] Z. Zhang et al., "Evaluation of Various Turbulence Models in Predicting Airflow and Turbulence in Enclosed Environments by CFD: Part 2—Comparison with Experimental Data from Literature", HVAC&R Research, 2007, vol. 13, no. 6:871–886.

[11] R. Zhao et al., "Heat Transfer in Upper Part of Electrolytic Cells-Part II: Heat and Flow Analysis and Correlations Based on CFD", Applied Thermal Engineering, (2012), (submitted).

[12] K. Rye, "Heat Transfer, Thermal Conductivity, and Emissivity of Hall-Heroult Top Crust", Light Metals 1995, (1995) p. 441–449.

[13] R. H. Perry et al., Perry's Chemical Engineers' Handbook, (McGraw-Hill New York, 1984), vol. 7.

[14] M. Taylor et al., "A dynamic model for the energy balance of an electrolysis cell", Chem. Eng. Res. & Design, 1996, vol. 74, no. 8:913–933.

[15] X. C. Shen et al., "Top Heat Loss in Hall-Héroult Cells", Light Metals 2008, (2008), 501-504.